Letters

A Novel Class-E Quasi-Constant Transconductance Rectifier

Haipeng Zhou and Qianyin Xiang, *Member, IEEE*

***Abstract*—A novel class-E rectifier with quasi-constant transconductance (QC-G_m) is proposed. The operation mechanism of the class-E QC-G_m rectifier is investigated, and the transconductance is calculated. The rectifier exhibits zero-voltage switching (ZVS) over a wide input and output range. The QC-G_m performance of a designed 40 mS rectifier is verified in a 6.78 MHz wireless power transfer link as demonstration. The rectifier is driven by constant voltage operation mode *LCC-LCC* network and class-E inverter, with unity overall dc–ac driving gain. The calculation matches the simulation, and the measurement shows that the output current is 0.96 A (±3.8%) under 25 V input voltage and 1–20 Ω loads.**

***Index Terms*—Quasi-constant transconductance (QC-G_m) class-E rectifier, wireless power transfer (WPT), zero-voltage switching (ZVS), load-independent.**

I. Introduction

CONSTANT-CURRENT (CC) power supply or drivers are required in battery powered devices and LED lighting systems. The conventional CC driving can be achieved by closed loop controlling [1], [2]. In recent years, CC topologies and class-D full-bridge rectifiers are used for CC driving [3]. This approach eliminates the need for complex closed-loop control, significantly simplifying the driving architecture, particularly in mid-to-low frequency WPT applications (e.g., hundreds of kHz). But its large number of switching/rectifying transistors introduces additional switching losses [1], [6], [7], [4]. With the rapid development of high-frequency, high-density integrated power electronic systems operating in the 6.78 MHz or higher frequency, class-E rectifiers have gained attention due to their zero-voltage switching (ZVS) characteristics and minimalist single-switch architecture, achieving efficiencies exceeding 95% under high-frequency operation [3], [2], [8], [9], [10], [11]. The application of class-E rectifiers in constant output topologies typically requires the input impedance of the rectifier to be independent of the load. The input to output current conversion ratio of traditional current-driven class-E rectifiers exhibits load-dependent variations [1]. Meanwhile existing research on load independent class-E rectifiers typically requires the active closed loop controlled synchronous switching devices [12]. Consequently, researchers have introduced closed-loop control strategies to maintain CC characteristics, but it increases system complexity, particularly in dynamic load scenarios where the robustness and real-time performance of control algorithms face significant challenges [2], [13].

In this letter, a novel class-E rectifier with quasi-constant transconductance (QC-G_m) performance is proposed. The rectifier achieves quasi constant transconductance characteristics through internal duty cycle adaptive adjustment mechanism. The dynamic equations and numerical solutions of the novel quasi constant transconductance rectifier are studied and verified. The class-E QC-G_m rectifier enables open-loop CC delivery to wide range loads, as well as ZVS operation. The working principle of the class-E QC-G_m rectifier is studied in Section II. In Section III, as a demonstration, the rectifier is driven by constant voltage (CV) operation mode *LCC-LCC* network and class-E inverter with unity overall dc–ac driving gain in a wireless power transfer (WPT) link, and the design equations and simulation results are given. The prototype measurement and the summary are given in Sections IV and V, respectively.

II. Mechanism of the QC-*GM* Class-E Rectifier

Fig. 1(a) illustrates the schematic of the proposed Class-E QC-G_m rectifier. C_1 is the parallel capacitor of the rectifier diode, which alternately conducts with diode D_1 to complete the periodic rectification process. L_{CG} acts as a constant transconductance inductor to dynamically adjust the transconductance of the rectifier under different load conditions. L_f and C_f form an *LC* low-pass filtering network to reduce output ripple waves, filter out high-order harmonic components for the dc output. For each operating cycle, the operation of the rectifier can be divided into two distinct operating states, i.e., OFF state and ON state, as shown in Fig. 1(b). In this configuration, u_{in} is the input ac voltage of the rectifier, u_R is the input voltage of the inductor, D_1 denotes the rectifying diode, the parallel-connected capacitor C_1 establishes a current path during the OFF state, the inductor L_{CG} converts the voltage from u_R into a stabilized current while serving as the rectifier's excitation source.

Received 19 April 2025; revised 24 May 2025; accepted 10 June 2025. Date of publication 13 June 2025; date of current version 5 August 2025. This work was supported by the National Natural Science Foundation of China under Grant 62371402. *(Corresponding author: Qianyin Xiang.)*

The authors are with the RF and Power Electronics Group, Institute of Microelectronics, School of Information Science and Technology, Southwest Jiaotong University, Chengdu 611756, China, and also with the Key Laboratory of Photonic-Electronic Integration and Communication-Sensing Convergence, School of Information Science and Technology, Southwest Jiaotong University, Chengdu 611756, China (e-mail: qyxiang@swjtu.edu.cn).

Color versions of one or more figures in this article are available at https://doi.org/10.1109/TPEL.2025.3579432.

Digital Object Identifier 10.1109/TPEL.2025.3579432

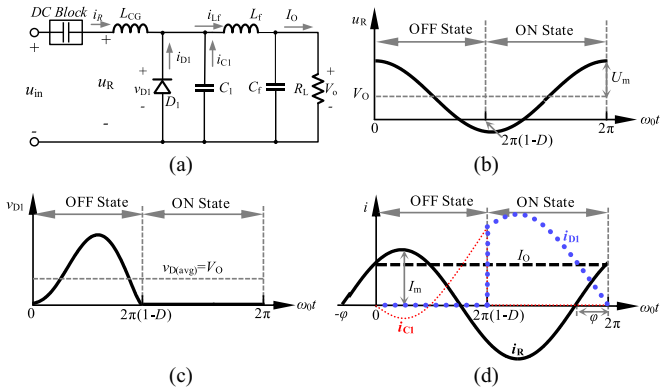

Fig. 1. Schematic and working waveforms of the class-E QC-G_m rectifier. (a) Schematic. (b) u_R. (c) v_{D1}. (d) i_{D1}, i_{C1}, i_R, and I_O.

In the OFF state, the diode D_1 is shutdown, and the voltage across the capacitor C_1 is equal to the reverse voltage of the diode. In the ON state, the diode D_1 is turned on due to the forward bias voltage reaching its threshold, and the voltage across the diode is clamped to the level of the forward voltage drop, i.e., $V_F \approx 0.2$–0.7 V. In this article, the V_F is set to zero for simplified analysis.

Due to the absence of dc part of the input current $i_R(t) = 1/L_{CG}\int[u_R(t)\text{-}v_{D1}(t)]dt$, the input voltage of the inductor can be written as $u_R(t) = u_{\text{in}}(t)\text{+}v_{D1(\text{avg})}$, where $u_{\text{in}} = U_m\cos(\omega_0 t\text{+}\varphi)$, $v_{D1(\text{avg})}$ is the average value of $v_{D1}(t)$, ω_0 is the working frequency, U_m is the amplitude of the $u_{\text{in}}(t)$, and φ represents the initial phase. Due to the low-pass filtering of the output network, the output voltage V_O is equivalent to the dc part of the Taylor series expansion of $v_{D1}(t)$, that is, $v_{D1(\text{avg})} = V_O$, as shown in Fig. 1(c). The input voltage of the inductor can be written as

$$u_R(t) = U_m\cos(\omega_0 t + \varphi) + V_O. \tag{1}$$

The current through the input inductor $i_R(t)$ contains multiple harmonic parts. The fundamental part can be considered for simplifying the analysis, and the rectifier input current is defined simply as

$$i_R(t) = I_m\sin(\omega_0 t + \varphi) \tag{2}$$

where I_m represents the amplitude of the input current, as shown in Fig. 1(d). According to the KCL, the output current i_{Lf} can be written as

$$i_{Lf} = i_R + i_{C1} + i_{D1} \tag{3}$$

where $i_{C1}(t)$ is the current of capacitor C_1, $i_{D1}(t)$ is the current of diode D_1. The diode is shut down in the OFF state, therefore, the current of the capacitor is zero at $t = 0$. At this moment, assuming the time constant of the output filter is large, the output dc current I_O can be given by

$$I_O = i_{Lf}|_{t=0} = I_m\sin\varphi. \tag{4}$$

In the OFF state, v_{D1} can be derived by (2), (3), and (4) as

$$v_{D1}(t)|_{t\in[0,(1-D)T]} = \frac{1}{C_1}\int i_{C1}(t)dt = \frac{I_m}{C_1}\int[\sin(\varphi) - \sin(\omega_0 t + \varphi)]\,dt$$
$$= \frac{V_O}{\omega_0 C_1 R_L}\left(\omega_0 t - \sin\omega_0 t + \frac{\cos\omega_0 t - 1}{\tan\varphi}\right). \tag{5}$$

In the ON state, $v_{D1} = 0$, therefore, V_O can be given by

$$V_O = \frac{1}{2\pi}\int_0^{T(1-D)} v_{D1}(t)dt$$
$$= V_O\begin{pmatrix}2\pi^2(1-D)^2 - \cos 2\pi D - 1\\ +2\pi(1-D)/\tan\varphi\\ +\sin(2\pi D)/\tan\varphi\end{pmatrix}/(2\pi\omega_0 C_1 R_L). \tag{6}$$

The duty cycle D is defined as the ratio of the turn-on time duration of D_1 to the total switching period T, and the load resistor $R_L = V_O/I_O$. To ensure the rectifier works in ZVS mode, the following condition must be satisfied:

$$v_{D1}(t)|_{t=(1-D)T} = 0 \tag{7}$$

From (2) to (7), it can be derived that

$$\tan\varphi = \frac{1-\cos(2\pi D)}{2\pi(1-D) + \sin(2\pi D)}. \tag{8}$$

Therefore, φ is an increasing function of D. The current and voltage of L_{CG} can be obtained from the volt-ampere relationship of the inductor as

$$i_R(t) = \frac{1}{L_{CG}}\int[u_R(t) - v_{D1}(t)]\,dt. \tag{9}$$

To simplify the calculation, the zero moment ($t = 0$) of the steady-state period is chosen to compute L_{CG}. Based on (1), (4), (6), (8), (9), and the initial condition of $i_{D1}|_{t=0} = i_{C1}|_{t=0} = 0$, $i_R|_{t=0} = I_O$, $v_{\text{D1}}|_{t=0} = 0$, and $u_R|_{t=0} = U_m\cos\varphi\text{+}V_{\text{O}}$, the solution is obtained as

$$\omega_0 L_{CG} = \frac{(U_m + V_O)\sin\varphi}{I_O} \tag{10}$$

where φ can be determined by (6) and (8). Referring to formula (10), this rectifier can reduce the value of L_{CG} by increasing the frequency. For specified V_{O}, U_m, ω_0, and L_{CG}, the output current I_{O} can be calculated by (6), (8), and (10), and the transconductance of the rectifier can be obtained as

$$G_{m\text{rec}} = I_O/U_m. \tag{11}$$

Fig. 2(a) shows the theoretical calculated $G_{m\text{rec}}$ versus the rectifier output voltage V_O under different values of L_{CG} when U_m is 25 V. Fig. 2(b) shows the $G_{m\text{rec}}$ versus the rectifier input voltage amplitude U_m under different values of L_{CG} when the output voltage is 10 V. According to Fig. 3, it shows that quasi-constant transconductance (QC-G_m) characteristics can be obtained over a wide range of input voltage, output voltage, and L_{CG}. The transconductance increases while L_{CG} decreases.

Based on the above theoretical analysis, Fig. 3 shows the design flow of the class-E QC-G_m rectifier.

1) In step 1, the rectifier capacitor C_1 can be calculated based on (6) and (8), with the given operating frequency, the typical load and its typical duty cycle. For $R_{L(\text{typ})} = 10\,\Omega$,

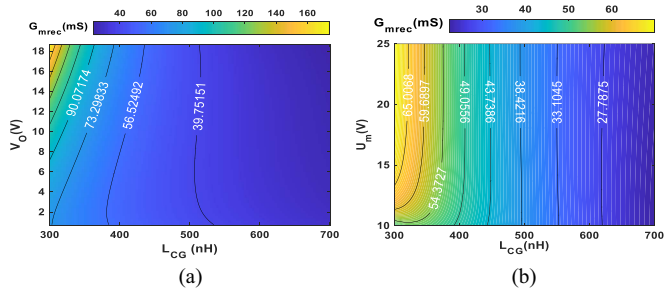

Fig. 2. (a) G_{mrec} versus Vo and L_{CG}, with $U_m = 25$ V. (b) G_{mrec} versus U_m and L_{CG}, with $V_O = 10$ V.

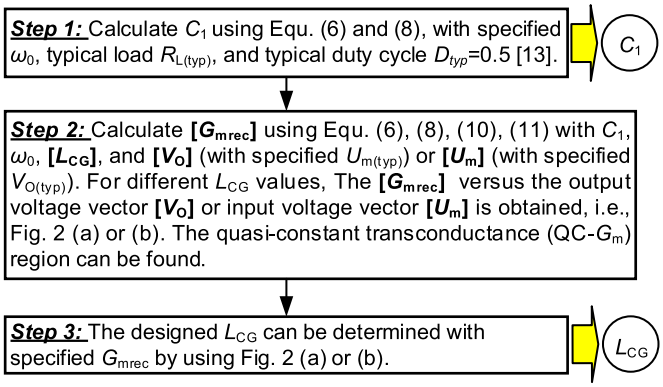

Fig. 3. Design flow of the class-E QC-G_m rectifier.

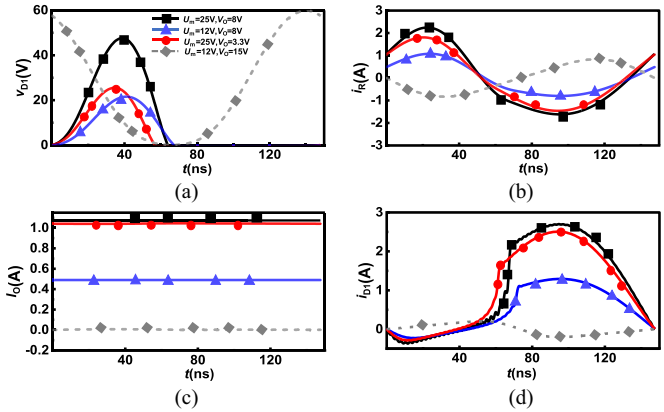

Fig. 4. Simulated working waveform of the rectifier. (a) V_{D1}. (b) Input current i_R. (c) Output current I_O. (d) i_{D1}.

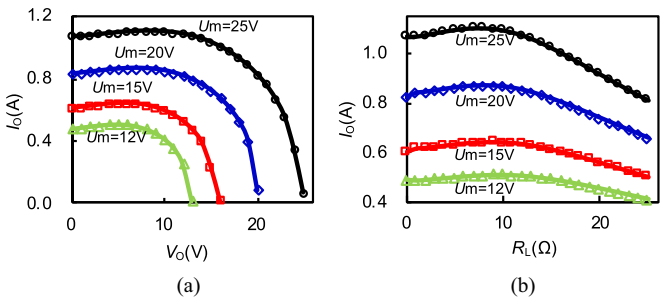

Fig. 5. I_O versus V_O. (a) Voltage load. (b) Resistance load.

$D_{(\mathrm{typ})} = 0.5$ [13], $\omega_0 = 2\pi \times 6.78 \times 10^6$ rad/s, the capacitor $C_1 = 500$ pF can be obtained.

2) In step 2, by using formulas (6), (8), (10), (11), and the C_1 obtained in step 1, the vector $[G_{mrec}]$ versus $[V_O]$ or $[U_m]$ can by calculated with different L_{CG}, and the quasi constant transconductance region can be found, as shown in Fig. 2(a) or (b).
3) In step 3, the L_{CG} can be determined with specified G_{mrec} based on the results in quasi constant transconductance region of Step 2. In the case of $G_{mrec} = 40$ mS, this article chooses $L_{CG} = 450$ nH.

Fig. 4 shows the simulated rectifier operating waveforms, where $L_{CG} = 450$ nH, $C_1 = 500$ pF, $L_f = 2$ μH, $C_f = 10$ μF, and the diode adopts PMEG100T080ELPE in Fig. 1. It shows that the following.

1) Comparing the curves (black, rectangle symbol) with $U_m = 25$ V, $V_O = 8$ V, and the curves (red, circle symbol) with $U_m = 25$ V, $V_O = 3.3$ V, for a specified U_m, the increases of V_O will lead to a reduction of the rectifier's duty cycle D and initial phase φ automatically as shown in Fig. 4(a),(b), and (d), where φ is defined in Fig. 1(d). By using (10), the reduction of φ will compensate the increase of V_O, and a quasi-constant output current I_O can be obtained for the specified U_m, as shown in Fig. 4(c). Therefore, a quasi-constant transconductance can be guaranteed.
2) Comparing the curves (black, rectangle symbol) with $U_m = 25$ V, $V_O = 8$ V, and the curves (blue, triangle symbol) with $U_m = 12$ V, $V_O = 8$ V, for a specified V_O, the increase of U_m will lead to an increase of the duty cycle D and rectifier's initial phase φ as shown in Fig. 4(a), (b), and (d). By using (10), the increase of φ will compensate to a larger output current I_O for the increase of U_m, as shown in Fig. 4(c), and a quasi-constant transconductance can be guaranteed.
3) For the curves (dash) with $U_m = 12$ V, and $V_O = 15$ V, it shows that the ZVS operation will be broken under a large output voltage, as shown in Fig. 4(a). This will suppress the turning on of rectifier diode, and the output current decreases, as shown in Fig. 4(c).

Fig. 5 shows the simulated curves of I_O under different input and output conditions. It can be observed that the rectifier is constrained by various factors, such as load, duty cycle, and diode performance, and exhibits constant transconductance characteristics under certain conditions. When the resistance-type load is used, the rectifier shows constant transconductance characteristics in the load range of 0–20 Ω. If the load range continues to increase, the transconductance of the rectifier will decrease, and the constant transconductance characteristics will gradually become worse. When the voltage-type load is used, the constant transconductance characteristics begin to deteriorate when the output voltage is close to the input amplitude U_m.

Fig. 6(a) shows the simulated rectifier efficiency under different input inductances and output voltages when $U_m = 25$

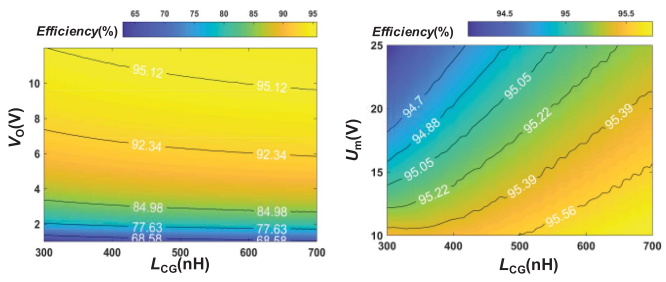

(a) (b)

Fig. 6. (a) Efficiency versus V_O and L_{CG}. (b) Efficiency versus U_m and L_{CG}.

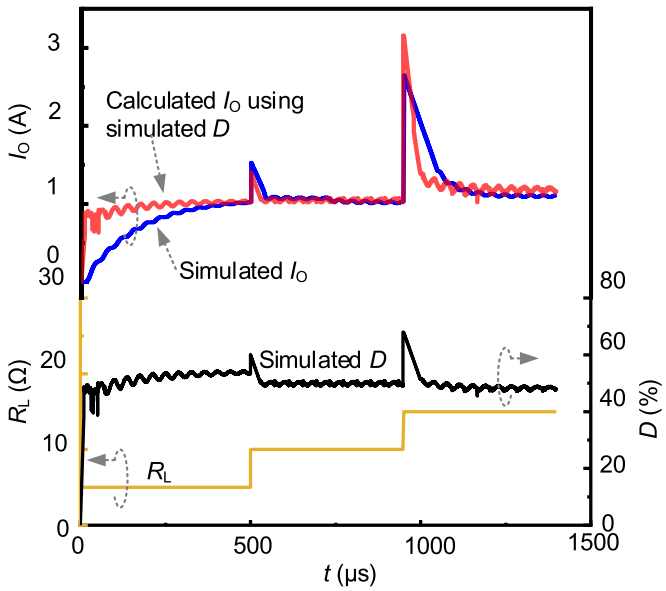

Fig. 7. Simulated load response of the duty cycle D, output current I_O, and the calculated I_O using the simulated duty cycle D.

V. When the output voltage is greater than 5 V, the rectifier efficiency exceeds 90%. Fig. 6(b) shows the rectifier efficiency under different input voltage amplitudes U_m, and input inductances when $V_O = 10$ V. It can be seen that the rectifier efficiency is affected by U_m slightly.

The load response simulation results are shown in Fig. 7. The load R_L is dynamically switched from 5 Ω to 10 Ω and 15 Ω, with a fixed input voltage amplitude $U_m = 25$ V, and operation frequency is 6.78 MHz. It can be seen that, the proposed Class-E QC-G_m rectifier can adjust the duty cycle automatically for achieving a constant output current I_O. The response of the duty cycle of the rectifier is extracted from the simulated data, the calculated output current I_O can be obtained by using (8) and (10), and the calculated I_O matches the simulated I_O very well as shown in Fig. 7.

III. Verification of the Class-E QC-*GM* Rectifier in a 6.78 MHz WPT Link

To verify the proposed class-E QC-G_m rectifier, a 6.78 MHz WPT link is designed as shown in Fig. 8. The rectifier is designed to be driven by a CV compensation network and class-E

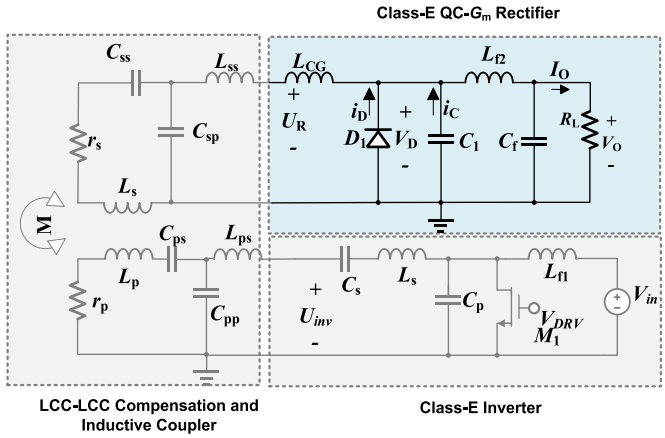

Fig. 8. WPT link for verifying the class-E QC-G_m rectifier.

TABLE I
Design Parameters of the WPT Link

Parameter	Value	Parameter	Value
V_{dc}	25 V	I_O	1 A
L_{PS}	0.83 μH	L_{ss}	0.5 μH
C_{PP}	490 pF	C_{SP}	810 pF
C_{PS}	100 pF	C_{SS}	98 pF
L_P	4.65 μH	L_{SS}	4.65 μH
r_p	0.8 Ω	r_s	0.8 Ω
R_L	1-20 Ω	C_P	500 pF
C_1	500 pF	D_1	PMEG100T080ELPE
M_1	GS66504b	M	1.6 μH

inverter with unity overall dc–ac gain for verification. Various CV compensation networks, such as *LCC-S*, *LCC-LCC*, can be used in practical designs to achieve the aforementioned function. CV mode *LCC-LCC* compensation network is chosen in the design [14]. The class-E inverter employs a CV inverter design that is independent of the load [15]. As a result, the input of the rectifier receives a CV independent of the load. The QC-G_m characteristics of the rectifier provide the load with a stable output current. Table I lists the component parameters of the WPT link

$$A_{\text{inv}} = \frac{V_{\text{inv}}}{V_{\text{in}}} = \frac{2q^2}{\pi(q^2-1)}\left[\sin(0.5\pi) + 0.5\pi\cos(0.5\pi)\right] = 3.5 \tag{12}$$

where V_{inv} is the magnitude of the inverter's output voltage, 0.5 is the duty cycle of the inverter, and q is the design constant of the inverter, which is independent of the load. In this article, q is taken as 1.25 [15].

The CV mode LCC-LCC compensation network consists of a high-order resonant network composed of a series compensation inductor L_{ps} and a capacitor C_{ps}, which realizes impedance conversion and improves load adaptability. The parallel compensation capacitor C_{pp} is used to improve the system quality factor (Q value) and frequency stability. The secondary side C_{ss}, L_{ss}, and C_{sp} have similar effects. The coil inductance L_p and L_s coupled with the mutual inductance M, and the internal resistances is r_p and r_s, respectively. The overall topology achieves CV output characteristics. By using the parameters in Table I, the voltage transfer gain of the *LCC-LCC* compensation network can be

TABLE II
COMPARISON OF PERFORMANCE BETWEEN THIS ARTICLE AND EXISTING RESEARCH

References	Frequency	Output Mode	Operating Range	Topology type
This article	6.78 MHz	CC with 0.965 A(±3.8%) @V_{in}=25 V	1−20 Ω or V_O=1 V – 20 V	Constant voltage topology + Class-E QC-G_m Rectifier (G_m = 40 mS by design)
Liu et al. [1]	6.78 MHz	CC with 1.05 A	13.3 – 16.5 Ω	Input dc voltage Control+SS/LC topology + Class-E Rectifier
Qu et al. [2]	200 KHz	CC with 1 A	10 – 30 Ω	Secondary closed loop control + Class-D Rectifier
Wang et al. [3]	85 KHz	CC with 1.04 A	24.36 – 40.8 Ω	*LC-S CC* topology + Class-D Rectifier
Komiyama et al. [4]	3.39 MHz	CC with 1.7 A	100 – 1 kΩ	Load independent Inverter + CC topology + Half-bridge Class-D Rectifier
Guo et al. [5]	85 kHz	CC with 2 A	5 – 50 Ω	Quasi-*LCC-S-S* topology + two channel Class-D rectifier, when the equivalent load is small

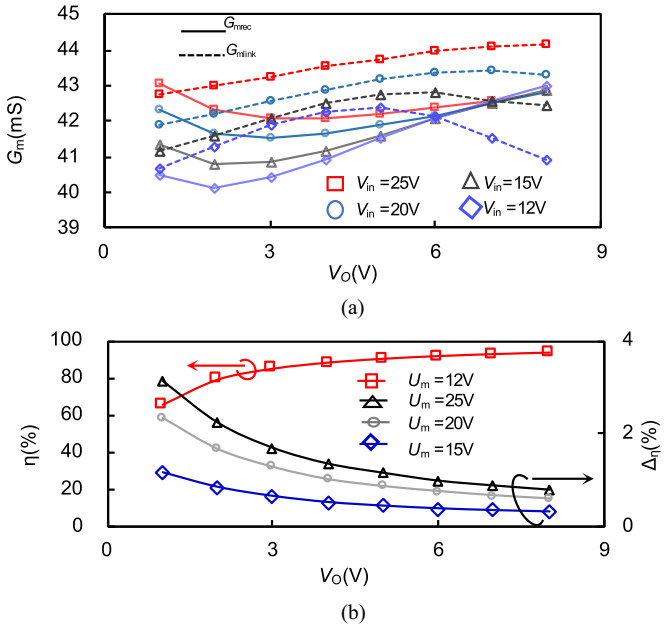

Fig. 9. (a) G_{mrec} and G_{mlink} versus V_O under different V_{in}. (b) Simulated efficiency of the rectifier under different U_m.

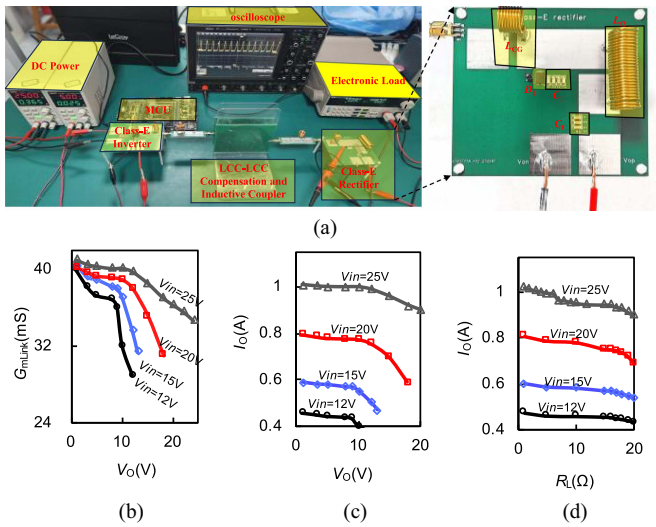

Fig. 10. Test configuration of the class-E QC-G_m Rectifier and measurement results. (a) Test configuration. (b) Overall transconductance of the WPT link G_{mlink}. (c) I_O under voltage load. (d) I_O under resistance load.

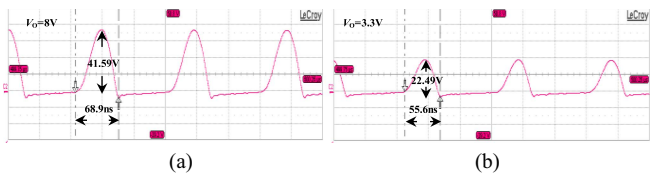

Fig. 11. Measured waveform of v_{D1}. (a) V_O = 8 V. (b) V_O = 3.3 V.

calculated as $A_{\mathrm{LCC}} = 0.3$ [14], and the transconductance of the rectifier can be calculated as $G_{mrec} = 40$ mS by using (11). Therefore, the transconductance of the WPT link can be derived as

$$G_{m\mathrm{link}} = A_{\mathrm{inv}} \cdot A_{\mathrm{LCC}} \cdot G_{mrec} \approx 40\mathrm{mS}. \tag{13}$$

Fig. 9(a) and (b) shows the simulated curves of G_{mrec} and $G_{m\mathrm{link}}$ versus output voltage V_O under different input voltages, as well as the efficiency curve of the rectifier under different output voltages, where the Δ_η is the difference between the rectifier efficiency under different input conditions (U_m = 25 V, 20 V, 15 V) and the rectifier efficiency when U_m = 12 V. The quasi-constant transconductance is verified by simulation.

IV. FABRICATION AND MEASUREMENTS

Fig. 10(a) shows the test configuration of the WPT system for verifying the proposed class-E QC-G_m rectifier. The LM5114B is used as the driver chip for the GaN transistors. The test is conducted using a LeCroy 104MXj-A oscilloscope and ZS1000 active probes. Fig. 10(b) shows the link transconductance $G_{m\mathrm{link}}$. of the system with a CV load. The measured typical $G_{m\mathrm{link}}$ = 41 mS when V_{in} = 25 V, meeting the design expectation of 40 mS. Fig. 10(c) shows the test results with CV load. The results indicate that the system can provide constant current charging for the CV load, the voltage-type load in the range of 1–20 V when V_{in} = 25 V. Fig. 10(d) indicates that, under the quasi-constant current operating mode, when the dc input voltage V_{in} = 25 V, the output current remains stable at I_O = 0.965A with a stability of ±3.8% as the load R_L dynamically varies within the range of 1–20 Ω. As given in Table II, compared with existing research, this new rectifier has a larger load-independent range than other literature. Fig. 11 shows the diode voltage waveforms under different output voltage conditions. It shows that the rectifier duty cycle is increased with the reduction of output voltage, which meets the design expectations as shown in Fig. 4(a).

V. Conclusion

A novel class-E QC-G_m rectifier is proposed. The rectifier dynamically adjusts transconductance through a duty cycle adaptive control mechanism, enabling the rectifier to achieve constant current output. The QC-G_{m} performance of the rectifier is verified in a 6.78 MHz WPT link. Prototype testing shows that, the output current variation rate is only 3.8% when the load changes from 1 to 20 Ω. It provides a new method to realize CC charging for constant resistance and CV loads.

References

[1] M. Liu, C. Zhao, J. Song, and C. Ma, "Battery charging profile-based parameter design of a 6.78-MHz class E^2 wireless charging system," *IEEE Trans. Ind. Electron.*, vol. 64, no. 8, pp. 6169–6178, Aug. 2017, doi: 10.1109/TIE.2017.2682017.

[2] X. Qu, Y. Jing, H. Han, S. C. Wong, and C. K. Tse, "Higher order compensation for inductive-power-transfer converters with constant-voltage or constant-current output combating transformer parameter constraints," *IEEE Trans. Power Electron.*, vol. 32, no. 1, pp. 394–405, Jan. 2017, doi: 10.1109/TPEL.2016.2535376.

[3] Y. Wang, Y. Yao, X. Liu, D. Xu, and L. Cai, "An LC/S compensation topology and coil design technique for wireless power transfer," *IEEE Trans. Power Electron.*, vol. 33, no. 3, pp. 2007–2025, Mar. 2018, doi: 10.1109/TPEL.2017.2698002.

[4] Y. Komiyama, A. Komanaka, W. Zhu, A. Konishi, K. Nguyen, and H. Sekiya, "Analysis and design of load-independent series resonant power amplifier with constant current output and its application for WPT system," *IEEE Trans. Power Electron.*, vol. 39, no. 5, pp. 6515–6525, May 2024, doi: 10.1109/TPEL.2024.3367373.

[5] D. Guo, W. Zhu, L. Hai, D. Li, and B. Cheng, "A novel dual-receivers/rectifier reconstructed WPT system with inherent CC to CV transmission characteristics and reactive power minimization," *IEEE J. Emerg. Sel. Top. Power Electron.*, early access, May 19, 2025, doi: 10.1109/JESTPE.2025.3571206.

[6] S. Aizawa, T. Yasuda, A. Uchida, W. Luo, X. Wei, and H. Sekiya, "Load-indenpendent class-E inverter with a class-D rectifier," in *Proc. 12th Int. Conf. Renew. Energy Res. Appl.*, 2023, pp. 279–282, doi: 10.1109/ICRERA59003.2023.10269364.

[7] H. Sekiya, K. Tokano, W. Zhu, Y. Komiyama, and K. Nguyen, "Design procedure of load-independent class-E WPT systems and its application in robot arm," *IEEE Trans. Ind. Electron.*, vol. 70, no. 10, pp. 10014–10023, Oct. 2023, doi: 10.1109/TIE.2022.3220818.

[8] X. Zan, Z. Guo, and A. T. Avestruz, "Inductive wireless power transfer at 100MHz with wide load range and constant output current," in *Proc. IEEE Energy Convers. Congr. Expo.*, 2019, pp. 4967–4975, doi: 10.1109/ECCE.2019.8912589.

[9] T. M. Tuan and W. Choi, "Design and implementation of a constant current and constant voltage wireless charger operating at 6.78 MHz," in *Proc. 10th Int. Conf. Power Electron. ECCE Asia*, 2019, pp. 1–6, doi: 10.23919/ICPE2019-ECCEAsia42246.2019.8797329.

[10] J. M. Arteaga, G. Kkelis, D. C. Yates, and P. D. Mitcheson, "A current driven class D rectifier with a resistance compression network for 6.78MHz IPT systems," in *Proc. IEEE Wireless Power Transfer Conf.*, 2016, pp. 1–4, doi: 10.1109/WPT.2016.7498794.

[11] X. Huang, Z. Yu, Y. Dou, S. Lin, Z. Ouyang, and M. A. E. Andersen, "Load-independent push–pull class E^2 topology with coupled inductors for MHz-WPT applications," *IEEE Trans. Power Electron.*, vol. 37, no. 7, pp. 8726–8737, Jul. 2022, doi: 10.1109/TPEL.2022.3150175.

[12] T. Mishima, S. Shimizu, and C.-M. Lai, "A load-independent ZVS class E^2 wireless power transfer with receiver-side constant-frequency PWM power control," in *Proc. 11th Int. Conf. Power Electron. Asia*, 2023, pp. 1038–1043, doi: 10.23919/ICPE2023-ECCEAsia54778.2023.10213964.

[13] T. Nagashima, X. Wei, E. Bou, E. Alarcón, M. K. Kazimierczuk, and H. Sekiya, "Steady-state analysis of isolated class E^2 converter outside nominal operation," *IEEE Trans. Ind. Electron.*, vol. 64, no. 4, pp. 3227–3238, Apr. 2017, doi: 10.1109/TIE.2016.2631439.

[14] Q. Zhu, L. Wang, Y. Guo, C. Liao, and F. Li, "Applying LCC compensation network to dynamic wireless EV charging system," *IEEE Trans. Ind. Electron.*, vol. 63, no. 10, pp. 6557–6567, Oct. 2016, doi: 10.1109/TIE.2016.2529561.

[15] L. Roslaniec, A. S. Jurkov, A. A. Bastami, and D. J. Perreault, "Design of single-switch inverters for variable resistance/load modulation operation," *IEEE Trans. Power Electron.*, vol. 30, no. 6, pp. 3200–3214, Jun. 2015, doi: 10.1109/TPEL.2014.2331494.